The optimization of a projectile from a three-coil reluctance launcher

Ferhat DALDABAN[1,*], Vekil SARI[2]
[1]Department of Electrical & Electronics Engineering, Erciyes University, Kayseri, Turkey
[2]Department of Electrical & Electronics Engineering, Cumhuriyet University, Sivas, Turkey

Abstract: This paper presents the design of a 3-coil reluctance launcher system and realization of an experimental prototype. A Maxwell model of the system was constructed and finite elements analysis (FEA) was applied before building the experimental prototype. The effect of variations in projectile parameters (such as material and length of the projectile) on projectile velocity was studied using the model. Then the experimental prototype of the launcher system was built. A velocity measurement system was also designed and implemented to measure the muzzle velocity of the launched projectiles. A total of 9 projectiles of 3 different sizes made of 3 different materials were constructed to be launched by the system. Each projectile was launched via capacitors charged with DC voltage between 50 and 200 V and the muzzle velocities were measured. Finally, the effects of projectile material and projectile length on muzzle velocity and launcher efficiency were examined. In this study, an easy-to-use, low-cost, portable, and structurally simple reluctance launcher that can be operated in relatively low voltage levels was implemented. Theoretical and experimental results were compared and it is concluded that the results are consistent with each other.

Key words: Coilguns, reluctance launchers, linear accelerators

1. Introduction

In recent years, there has been an important increase in studies on electromagnetic launchers. Electromagnetic launchers can be used in many different areas such as military, space, air, sea, and industrial applications [1]. The structure and operation of electromagnetic launchers are similar to those of linear motors except railguns. Linear motors are used in high speed transportation systems, electric hammers, electrochemical pumps, and many electromechanical systems [2]. It can be used in linear motors, elevators, self-opening doors etc. [3], and it can also be used to change railway channels [4]. Electromagnetic launchers can be examined in two main categories according to their operation style. These are electromagnetic railguns and electromagnetic coilguns [5]. Electromagnetic railguns consist of two parallel rails, a conductor that contacts with the rails and provides the current flow between two rails, and a projectile to be launched. The current loop is completed by means of a conductor that can move between the rails [6]. Because this conductor is inside a magnetic field, a force is induced on it. Then the conductor fastens and launches the projectile in front of it. When compared to an electromagnetic coilgun, an electromagnetic railgun has a higher projectile speed and it is more efficient, but the required current is very high [7]. Electromagnetic coilguns consist of a coil wound on an empty cylinder, and a projectile [8]. In electromagnetic coilguns, there is almost no friction between the barrel and the projectile. Thus the acceleration system is not harmed [9]. Electromagnetic coilguns can be studied in two main categories

---

*Correspondence: daldaban@erciyes.edu.tr

according to their operation principles. These are induction launchers and reluctance launchers. In induction launchers, the nonmagnetic projectile is fastened and launched by pushing it with the use of the magnetic field on the coil. The induction launcher is related to the eddy currents induced on the core [10]. The induction launcher uses the Lorentz force to fasten the projectile with a conducting armature [11]. The reluctance launcher has the same operation principle with reluctance motors [12]. In the reluctance launcher the ferromagnetic projectile is out of the coil and is pulled to the middle of the coil using the magnetic field; it is not pushed. When compared to the induction launcher, its efficiency is better and launching can be satisfied in smaller currents [13].

It is difficult to evaluate the performances of reluctance launchers due to the nonlinearity of B–H characteristics of the ferromagnetic materials. Finite element analysis (FEA) can be used for this purpose. FEA is a numerical analysis method that is successfully used in the analysis of engineering problems that cannot be solved or are difficult to solve by using classical methods. Therefore, 2D and 3D FEA have been used to evaluate the performance of reluctance launchers in earlier studies [10,14,15]. In this study, 2D FEA is used to analyze the proposed launcher system.

2. Structure of a reluctance launcher

A simple reluctance launcher with one winding has three parts as given below:

1. Barrel: An empty, nonmagnetic pipe,

2. Winding (Coil): A winding wound around the barrel (stator winding),

3. Core (Projectile): A ferromagnetic, cylindrical simple core to be launched.

Parts of a reluctance launcher are shown in Figure 1. When a current flows through the winding, a magnetic field occurs around the winding as shown in Figure 1. When a ferromagnetic core exists inside the barrel and close to the winding, magnetic flux will try to complete its loop on the core because the permeability of the core is much more than that of the air. As a result, the magnetic flux applies a force to the core to reduce the reluctance of the environment and moves it to the center of the winding [1].
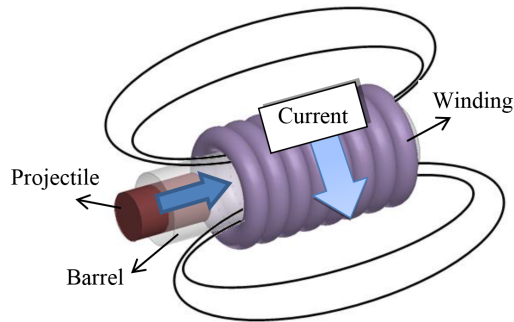
Figure 1. Parts of a reluctance launcher and the magnetic field due to the flowing current.

A reluctance launcher is actually an electromechanical converter where the electrical energy of the electrical source is converted to magnetic and mechanical energy as given in Eq. (1).

$$dW_e = dW_m + dW_f, dW_e = dW_m + dW_f \tag{1}$$

where dWe, dWm, and dWf are the rise in electrical energy (except the lost energy) transferred to the system, the energy converted to mechanical energy, and the energy stored in the magnetic field during a time interval of dt, respectively.

While some of the electrical energy is stored in the magnetic field, some of it is converted to mechanical energy if the losses are ignored.

If the movement is at the constant current conditions, the mechanical work done is the increase in the coenergy. Therefore,

$$dW_m = dW_f'$$ (2)

can be written.

The coenergy is the area between the current-axis and the trajectory at the flux linkage–current characteristic trajectory and is given as below:

$$W_f' = \int\limits_0^i \lambda di,$$ (3)

where i and λ are the current applied to the winding and the flux linkage occurring at the winding, respectively. Flux linkage–current characteristics can be written as follows for the linear condition:

$$\lambda = L(x)i,$$ (4)

where L(x) is the inductance of the winding. From (3) and (4) coenergy can be given as for the linear system.

$$W_f = W_f' = \frac{1}{2}L(x)i^2$$ (5)

If the force causes the projectile to displace as much as dx is f_m,

$$f_m = \frac{\partial W_f'(i,x)}{\partial x}?_{constant\ i}$$ (6)

can be written. As a result, the force is given by using (5) and (6) as below [16].

$$f_m = \frac{\partial}{\partial x}\left(\frac{1}{2}L(x)i^2\right)?_{constant\ i} = \frac{1}{2}i^2\frac{dL(x)}{dx}$$ (7)

The magnetic field occurring at the winding moves the core through the center of the winding as shown in Figure 1. Reluctance launchers work according to the principle of pulling the core to the center of the winding and the core is not pushed [17]. When the core is at the center, the energy of the winding must be cut off and the energy inside should be damped in the shortest time. Otherwise, the core cannot be launched or is slowly launched because the core will again be pulled to the center of the winding. This is the most critical point in the design of the reluctance launcher. Therefore, a sensor is necessary, which perceives that the core has come to the center of the winding.

If the reluctance launcher consists of more than one winding, each winding affects the core when it is energized. In this system, the critical point is the timing. When the core approaches the next winding, then that winding should be energized and the energy should be cut off when it comes to the center of the winding and the energy of the winding should be damped at the shortest time. The efficiency of the reluctance launcher

depends on the timing of the current flowing through the windings and timing of the damping of the energy at the windings.

The timing of applying and cutting off the energy can be realized by placing an optical receiver–transmitter pair at the entrance of the winding as shown in Figure 2.
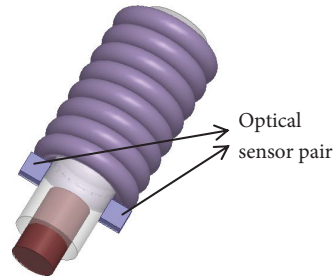
Figure 2. Placement of the optical sensor pair.

The reluctance launcher operation is similar to that of the reluctance motor. Reluctance can be defined as the resistance against magnetic field and is expressed as follows [1]:

$$\Re = \frac{l}{\mu_r \mu_0 A},$$ (8)

where

l : length of the magnetic path (m)

μ_r : relative magnetic permeability of the material

μ_0 : permeability of air (H/m)

A : cross-sectional area where magnetic flux flows (m^2)

In the reluctance coilgun, almost all of the reluctance is observed at the air gap between the projectile and the driving coil. Here air gap g is two times the existing gap $(l = 2g)$, because the flux lines pass through this gap twice. When the projectile reaches the center of the coil, area A will be equal to half of the cylindrical plane with a diameter of d and a length of p $(\pi dp/2)$. Then Eq. (8) is as follows:

$$\Re = \frac{4g}{\mu_0 \pi \, d \, p},$$ (9)

where

g : air gap between the projectile and the coil

μ_r : 1 for air

μ_0 : permeability of air

p : diameter of muzzle

p : length of the projectile

The projectile moves through the center of the coil where reluctance is minimum. The force applied to the projectile by the coil can be determined using the classical electromagnetic theory [12]. Let us assume that a projectile with constant permeability is put along the spiral axis of a very long coil. To calculate the force applied to the projectile, we need to calculate the difference in the system energy when the projectile moves

Δx. Then the difference in the system energy is expressed in Eq. (10).

$$\Delta W = \frac{1}{2} \int_{A.\Delta x} , (\mu - \mu_0) H^2 dV \tag{10}$$

The force generated by the reluctance launcher is defined by Eq. (6). Finally the acceleration of the projectile is given by Eq. (11).

$$a = \frac{\mu_0(\mu_r - 1)(NI)^2 A}{2ml^2}, \tag{11}$$

where

      N: number of coil turns

      I: current flowing through the coil

      A: cross-sectional area of the coil

      M: mass of the projectile

      l: length of the coil

According to Eq. (11), acceleration of the projectile is directly proportional to the projectile's relative permeability, square of the current flowing through the coil, and cross-sectional area of the coil, whereas it is reversely proportional to the mass of the projectile and square of the length of the projectile.

To calculate the magnetic field inside the coil, let us consider an N-turns coil of length l and radius a with a current of I flowing through it as shown in Figure 3.
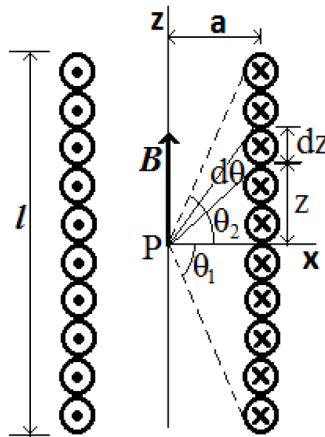

Figure 3. Cross-section of the coil.

To determine the magnetic flux density on a point P that lies on the coil-axis, first we need to write the expression of magnetic field H at a distance of z from the center of a ring having a radius of a [18].

$$H = \hat{z} \frac{I' a^2}{2(a^2 + z^2)^{3/2}} \tag{12}$$

Here I' is the current flowing through the ring. If we assume a small coil-length dz as an equivalent ring having ndz turns and carrying a current of $I' = Indz$, then the field induced at point P is as follows:

$$dB = \mu dH = \hat{z} \frac{\mu n I a^2}{2(a^2 + z^2)^{3/2}} dz \tag{13}$$

Total magnetic field B at point P is calculated by summing all the contributions from the entire coil. Then B at point P is defined by Eq. (14).

$$B = \hat{z}\frac{\mu nI}{2}(sin\theta_2 - sin\theta_1) \tag{14}$$

3. FEA of the reluctance launcher system

FEA of the proposed single-winding launcher system is realized by using Ansys Maxwell software. A two-dimensional cylindrical z-axis is chosen in the model analysis and a geometry that belongs to this axis is built. To reach the fastest projectile velocity, materials of the projectiles and their lengths have been changed for the analysis. 2D and 3D models of the system are shown in Figures 4 and 5, respectively.
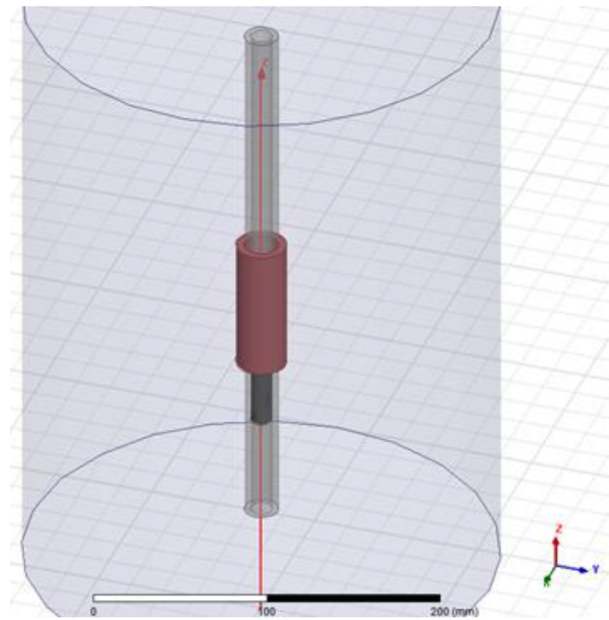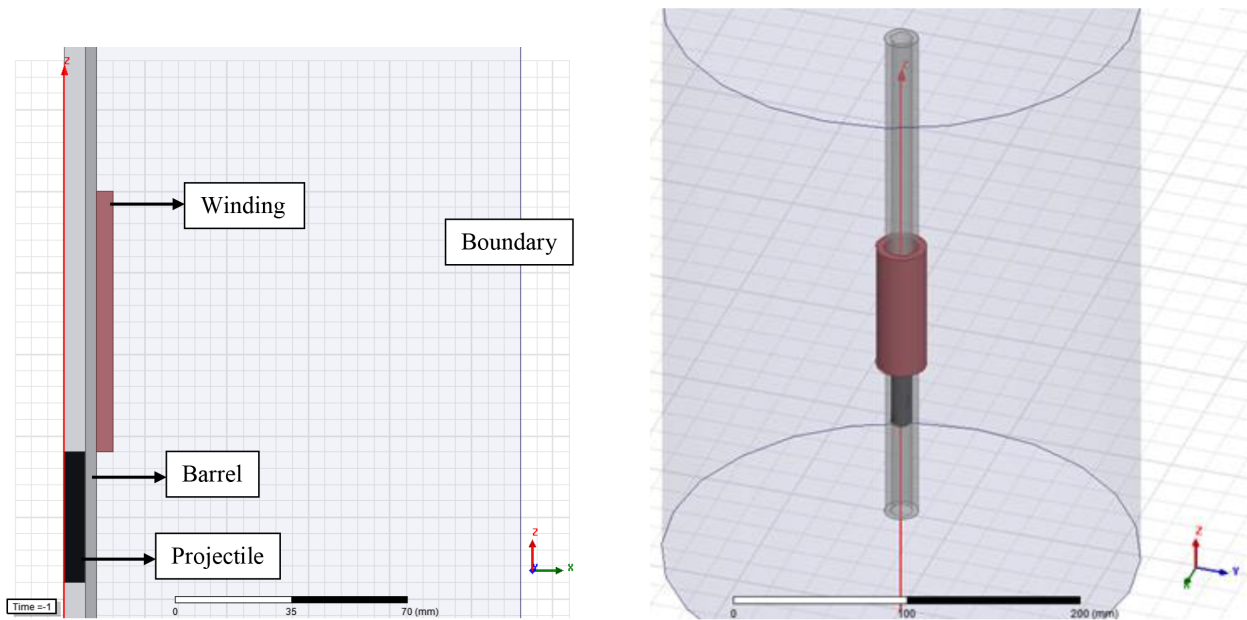
Figure 4. 2D Maxwell model of the reluctance launcher.

**Figure 5.** 3D Maxwell model of the reluctance launcher.

Projectiles having a diameter of 12.5 mm and length between 1 and 10 cm constructed from 3 different materials (AISI1020, AISI1050, and AISI12L14) were analyzed in terms of the projectile velocity. The results are shown in Table 1.

Figure 6 shows the velocities according to projectile length. In terms of the projectile material, the maximum velocity is achieved using projectiles built from 1050 material, then comes the projectiles built from 12L14, and the minimum velocity is achieved using projectiles built from 1020. In terms of projectile length, all projectiles built with different materials reach the maximum velocity at 4 cm length. The projectile velocity decreases as the projectile length increases. The maximum velocity is 19.86 m/s using the constructed model. This value is obtained with a 4-cm length projectile built from 1050 material.

Maximum velocity becomes 19.86 m/s within 9.6 ms as shown in Figure 7. When the projectile reaches the maximum velocity, the winding energy should be cut off. Otherwise the projectile will slow down and then the winding will pull it to its center again. This situation is shown for the position of the projectile and the force applied to the projectile in Figures 8 and 9, respectively.

Table 1. Velocity results (m/s).

Projectile length (cm)	Projectile mass (g)	Projectile type		
		1020	1050	12L14
1	7.5	15.57	15.59	15.58
2	17	17.66	18.11	17.85
3	26.5	18.62	19.05	18.86
4	36	19.36	**19.86**	19.60
5	45.5	19.11	19.8	19.56
6	55	19.06	19.76	19.41
7	64.5	18.92	19.51	19.20
8	74	18.79	19.25	18.95
9	83.5	18.32	18.87	18.54
10	93	17.78	18.4	18.11
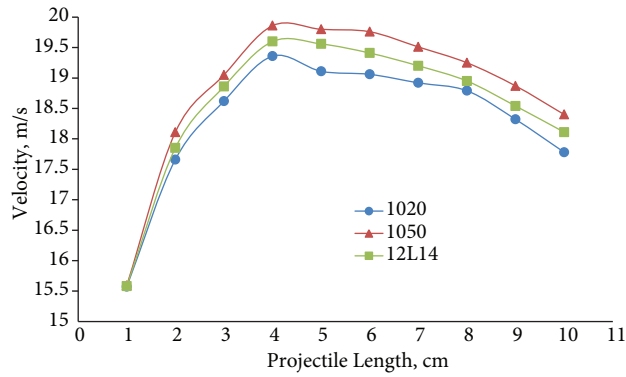
Figure 6. Velocity–projectile length graph.
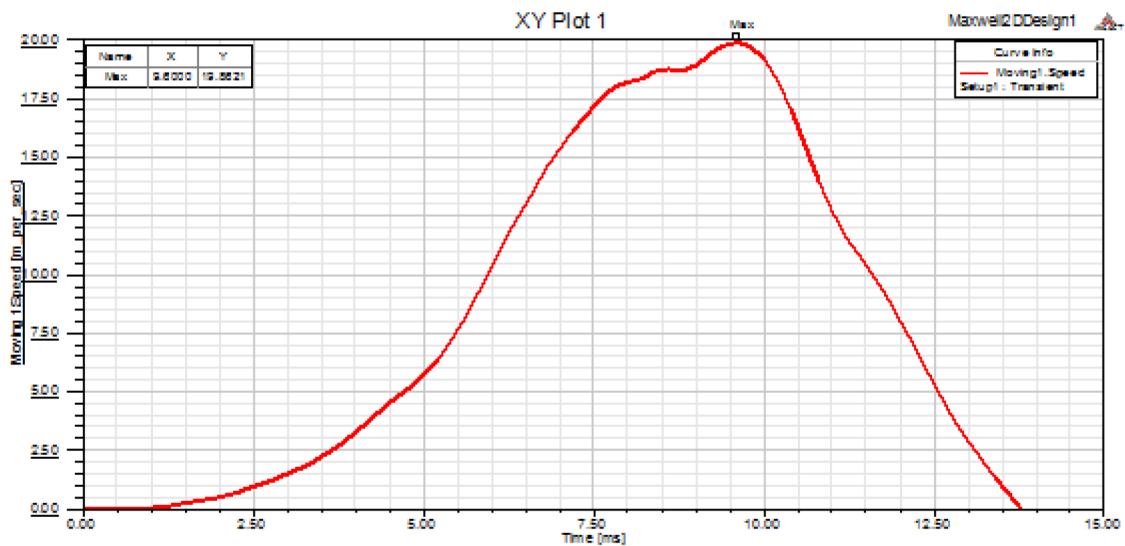
Figure 7. Velocity–time graph of the 4-cm 1050 projectile.
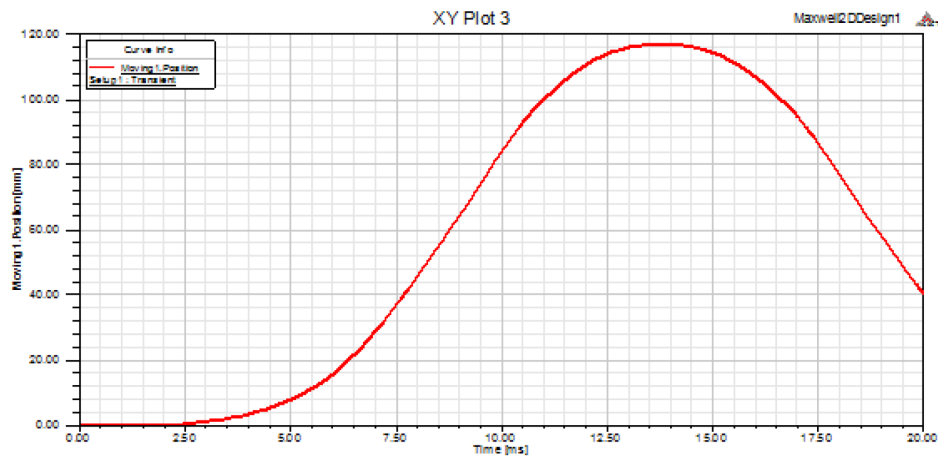
Figure 8. Position–time graph of the 4-cm 1050 projectile.
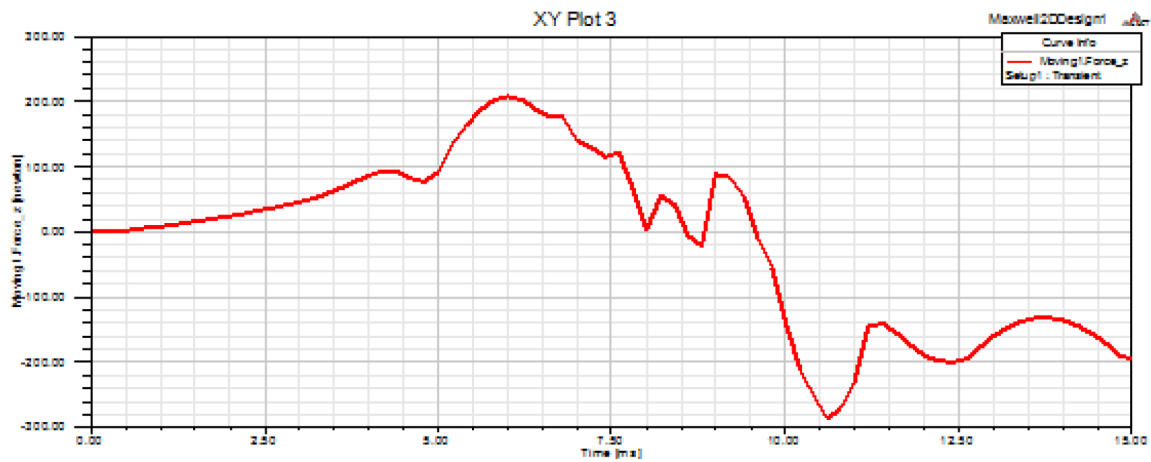

Figure 9. Magnetic force–time graph of the 4-cm 1050 projectile.

The projectile got out of the sensors when it reached its maximum speed and the energy in the windings should be damped quickly. Otherwise, the projectile will be pulled back as shown in Figure 8. In addition, when the force affecting the projectile is maximum, the velocity also becomes maximum. If the winding energy is not cut off after the projectile reaches its maximum, then the magnetic force applied to the projectile becomes maximum in the opposite direction as shown in Figure 9.

Magnetic flux lines and the magnetic flux density are also examined in the reluctance launcher system model. Figure 10 shows the distribution of the magnetic lines when the projectile reaches maximum velocity and Figure 11 shows the magnetic flux density for the same situation.

Figure 12 shows that coil flux is at maximum when the projectile reaches the maximum velocity. At that point the value of the coil flux is 0.29 Webers.

4. Experimental work

A reluctance launcher system with three windings is realized for experimental studies. The system has five main parts which are the mechanical structure, the power supply, the control unit, the driver unit and the velocity measurement system.Three windings are shown in Figure 13.
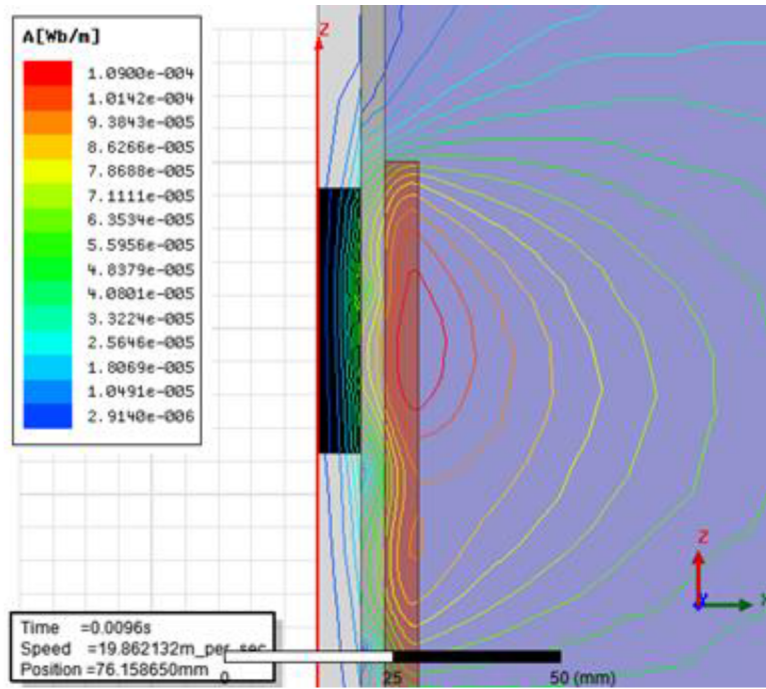
Figure 10. Distribution of magnetic flux lines when the 4-cm 1050 projectile reaches maximum velocity.
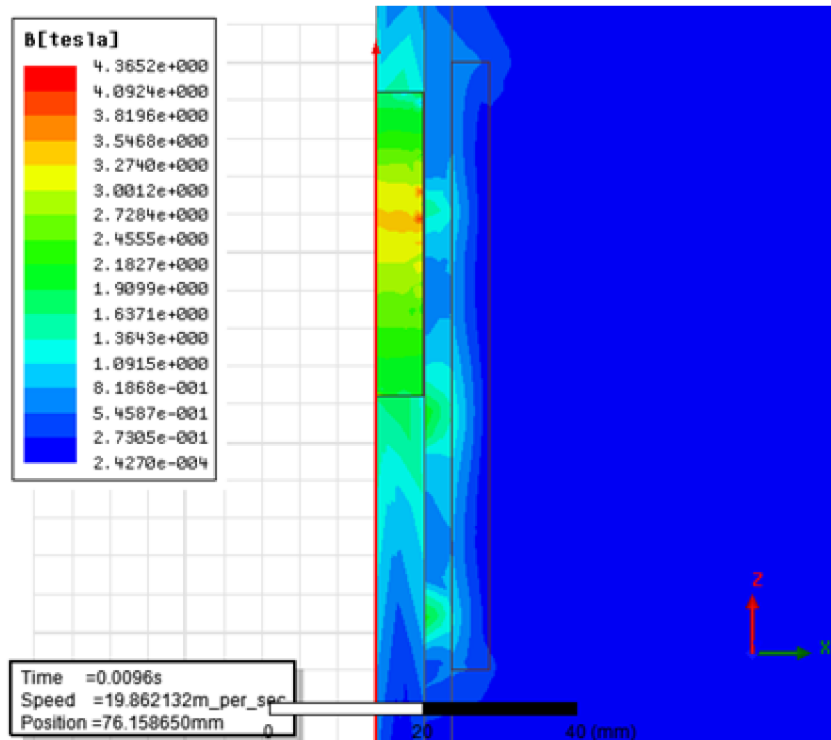

Figure 11. Distribution of the magnetic flux density when the 4-cm 1050 projectile reaches maximum velocity.

The mechanical structure consists of three windings, three optical sensor pairs at the entrance of the each winding, and two optical sensor pairs 18 cm away from each other to measure the projectile velocity. The

windings are constructed from 0.8 mm^2 wires wound for 540 turns. The lengths of the windings is 8 cm, the inner gap is 20 mm, and the height is 5 mm. Dimensions of the mechanical part of the system are shown in Figure 14.
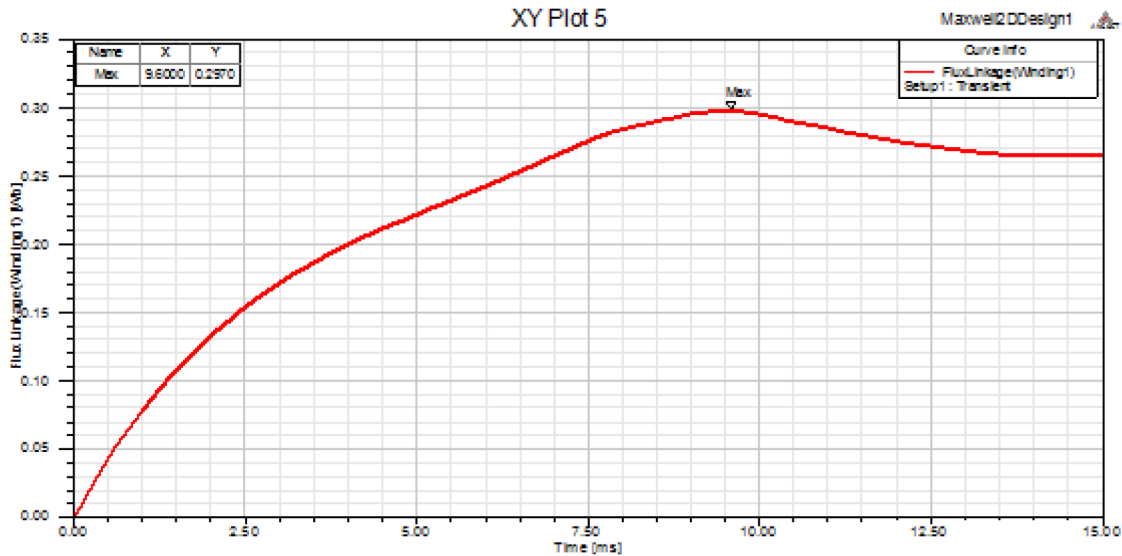

Figure 12. Magnetic flux–time graph.
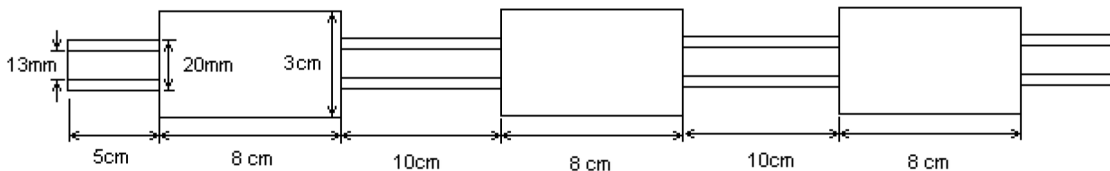

Figure 13. Three-coil reluctance launcher.

Figure 14. Dimensions of the mechanical structure.

The power supply of the system consists of eight 2700 μF capacitors and launching is done by charging these capacitors. The control unit includes IGBT driver circuits. Triggering signals of the IGBTs are generated by using signals obtained from the optical sensors. The driver unit has three IGBTs and snubber circuits. The related winding is energized via IGBTs, which are taken into transmission mode for a necessary duration by using the IGBT triggering signals obtained from the control unit.

A circuit schema of the reluctance launcher is shown in Figure 15. The photo transistor is in active-state when there are no projectiles between the optical sensor pair. In this case zero voltage is seen on the driver input and the IGBT does not switch to the active state because of zero volts on the driver output. When the projectile passes through the optical sensor pair, it prevents light and the photo transistor switches to the cut-off state. In this situation, the supply voltage is applied to the input of the driver, and it is also applied to the IGBT's gate from the output of the driver. Then the IGBT switches to the active state and collector–emitter

path is short-circuited. The coil is the load in the collector–emitter circuit. When the collector–emitter is short-circuited, eight 200-V charged, parallel connected 2700 μF/500 V capacitors are also short-circuited through the coil. A magnetic field is induced by the current flowing through the coil. When the projectile prevents the sensor, it is close to the coil and enters the attraction zone of the coil. Therefore it is pulled to the center of the coil with the effect of the induced magnetic field.
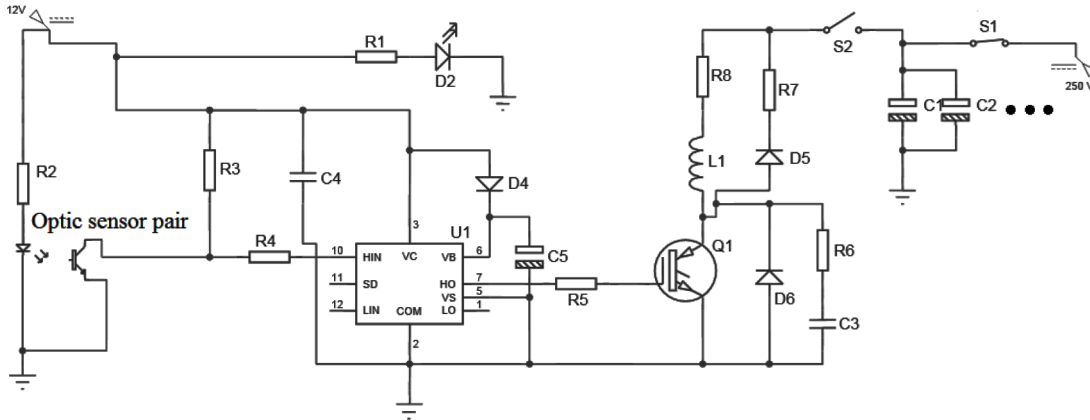

Figure 15. Circuit schema of the reluctance launcher.

When the projectile gets to the center of the coil, it gets out of the way of the sensors and the transistor switches to the active state. Thus the system gets to the initial state and the IGBT switches to the cut-off state. The energy applied to the coil is interrupted, but it does not decrease immediately. The inductive current keeps flowing through. This energy is discharged by the diode and the resistance, which are parallel connected to the coil.

The velocity measurement system measures the muzzle velocity of the projectile by using the optical sensors positioned for velocity measurement. A block diagram of the velocity measurement part is shown in Figure 16.
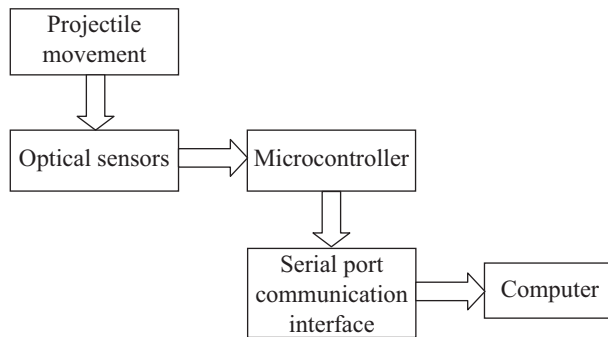

Figure 16. Block diagram of the velocity measurement system.

The velocity measurement system consists of four different parts: optical sensors, microcontroller, serial port communication interface, and software. The velocity measurement system was implemented using the interrupt mode of the PIC16F876 microcontroller. The signal that is produced while the projectile is getting through the sensors was applied to the microcontroller. The time between two signals is calculated using the

internal counter (TMR1). TMR1 consists of two 8-bit registers that are both readable and writable and are called TMR1H and TMR1L. Then the velocity can be calculated in m/s by dividing the distance between the sensors (18 cm).The movement of the projectile is sensed by the sensors, the signal produced by two separate sensor pairs has two rising edges, and it is applied to the microcontroller. The microcontroller calculates the duration of the projectile transition between two sensor pairs with a counter. This time information is transferred to the computer via a serial port interface. The software, written in Visual Basic programming language, calculates the velocity by dividing the distance between two sensors by the calculated time.

Nine projectiles were constructed in three different lengths from three different materials to be launched by the system. The first material is known as transmission steel in industry with the code 1020. The second material is known as construction steel with the code 1050. Finally, the third material is known as automat steel with the code 12L14. Figure 17 shows the projectiles used.

Figure 17. Projectiles used.

Dimensions of the projectiles are shown in Table 2. Table 3 shows the codes of the materials used in standards of other countries. Transmission steel gets its name from the carbon percentage it contains. It contains 0.20% of carbon, which gives it the code name 1020. Similarly, construction steel contains 0.50% carbon, and thus is named 1050. Automat steel also includes lead among carbon and other elements. Table 4 shows the chemical contents of the projectile materials [19]. Carbon percentage is between 0.18% and 0.25% for AISI 1020 steels. All the steels that have a carbon percentage between these values are called 1020 steel. This difference in carbon percentage depends on the manufacturer itself. The rest of the compounds in all steel types is iron. 1020 has the highest iron rate and then comes 1050 and 12L14 in that order.

Table 2. Dimensions of the projectiles.

Material type	Projectile diameter	Projectile length			Total
Transmission steel, 1020	1.25 cm	4 cm	6 cm	8 cm	3
Construction steel, 1050	1.25 cm	4 cm	6 cm	8 cm	3
Automat steel, 12L14	1.25 cm	4 cm	6 cm	8 cm	3
Total		3	3	3	9

Table 3. Equivalents of projectile materials in standards of other countries.

Equivalents in standards of other countries							
Germany DIN 17210		France	UK	Italy	Japan	CIS	USA
Material no.	Symbol	AFNOR	B.S.	UNI	JIS	GOST	AISI/SAE
1.0402	C 22	AF 42 C 20	050 A 20	C 20 ; C 21	-	20	1020
1.1213	Cf 53	XC 48 H1 TS	060 A52; 070 M 55	C 53	S50C	50	1050
1.0737	9 SMnPb 36	S 300Pb	-	CF 9 SMnPb 36	-	-	12L14

Table 4. Chemical compound rates of projectile materials.

| Chemical compound (% mass)						
Code	C	Si	Mn	P_{max}	S_{max}	Pb
1020	0.18–0.25	0.15–0.35	0.30–0.60	0.045	0.045	–
1050	0.50–0.57	0.15–0.35	0.40–0.70	0.025	0.035	–
12L14	0.57–0.65	0.10–0.40	0.50–0.90	0.060	0.15–0.25	0.20–0.35

5. Experimental results

First of all, projectiles of length 4 cm, 6 cm, and 8 cm constructed from 1020 material were launched at voltage levels between 50 and 200 V. Figure 18 shows the velocities of the projectiles.

Then projectiles of length 4 cm, 6 cm, and 8 cm constructed from 1050 material were launched at voltage levels between 50 and 200 V. Figure 19 shows the velocities of the projectiles.
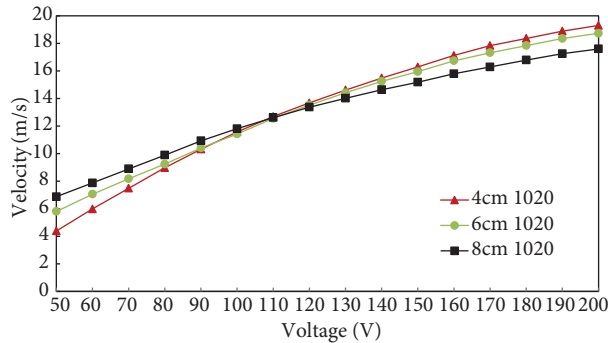
Figure 18. Velocities of projectiles constructed from 1020 material and having lengths of 4 cm, 6 cm, and 8 cm.
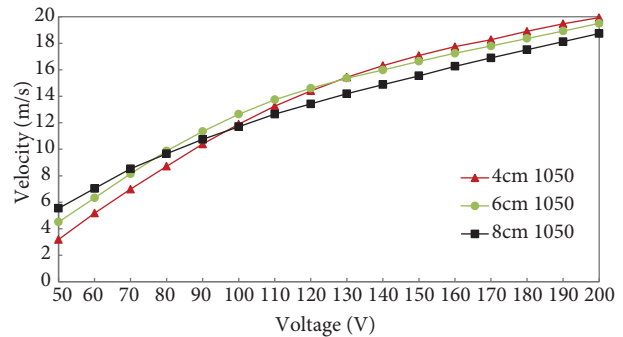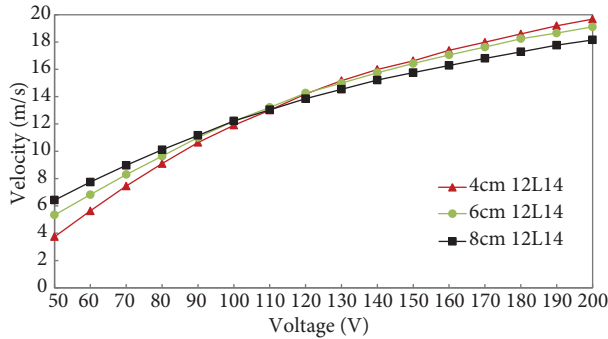
Figure 19. Velocities of projectiles constructed from 1050 material and having lengths of 4 cm, 6 cm, and 8 cm.

Finally projectiles with the same lengths constructed from 12L14 material were launched at voltage levels between 50 and 200 V. Figure 20 shows the velocities of the projectiles.

When Figures 18, 19, and 20 are compared, it can be seen that the 4-cm-length projectile is slower than the other projectiles at lower voltage levels. When the applied voltage increases, the 4-cm projectile has a higher velocity than the other projectiles and it reaches the maximum velocity at 200 V. This can be explained by the acceleration expression in Eq. (11). Acceleration of the projectile is directly proportional to the square of the current flowing through the coil and reversely proportional to the mass of the projectile. Because the current will be small at low voltage levels, the latter effect will be higher than the former and the projectile velocity will be relatively small. When the applied voltage increases, the current flowing through the coil also will increase. The effect of the increase in current will be higher than that of the decrease in the projectile mass and then velocity will increase too.

Using these velocity results, the velocities of the projectiles constructed from various materials should be summarized together. Figure 21 shows the velocities of 4-cm-length projectiles with different materials, Figure 22 shows the velocities of 6-cm-length projectiles with different materials, and Figure 23 shows the velocities of 8-cm-length projectiles with different materials.
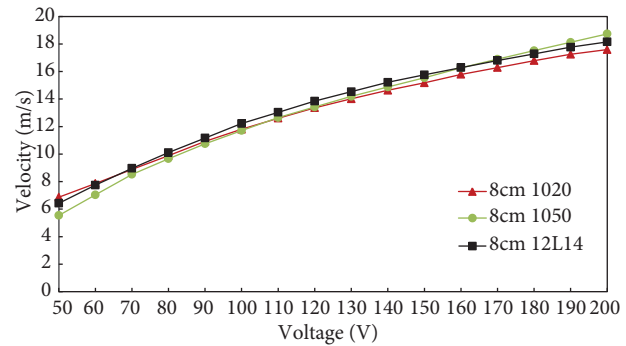

Figure 20. Velocities of projectiles constructed from 12L14 material and having lengths of 4 cm, 6 cm, and 8 cm.
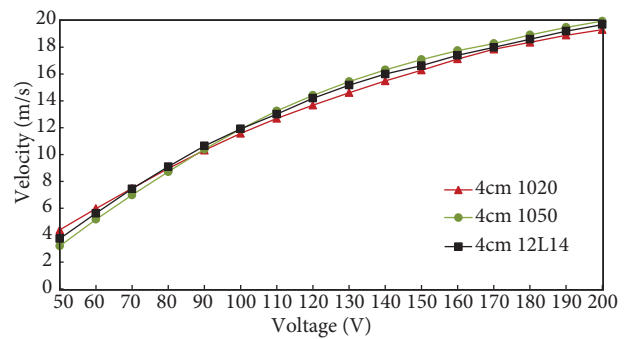
Figure 21. Velocity graph for 4-cm-length 1020, 1050, and 12L14 projectiles.
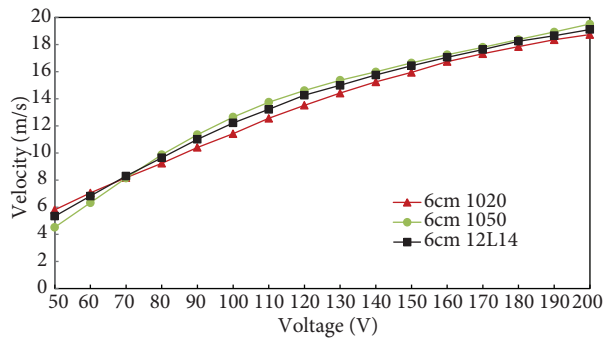

**Figure 22.** Velocity graph for 6-cm-length 1020, 1050, and 12L14 projectiles.

Figure 23. Velocity graph for 8-cm-length 1020, 1050, and 12L14 projectiles.

When we examine Figures 21, 22, and 23, it can be seen that projectiles constructed with 1020 material have higher velocities at lower voltages and have minimum velocities at 200 V. This is because of the lower magnetic fields at lower voltage levels. It can be understood from Figure 24 that 1020 has a high permeability when the magnetic field is low. Then when a higher voltage is applied, a higher magnetic field occurs and 1020's permeability becomes lower than the others. Muzzle velocity is directly proportional to the permeability. Thus, at lower magnetic field levels (lower voltage levels), projectiles constructed from 1020 will have higher velocities and vice versa.

Velocities at 200 V are shown in Figure 25. The 4-cm-length projectiles reach the highest velocity among three different-length projectiles in each of the three materials. This is consistent with the acceleration expression in Eq. (11) because the acceleration is reversely proportional to the projectile mass. The lightest projectile should be the fastest one. If the projectile length is increased while the other parameters are held constant, projectiles get slower.
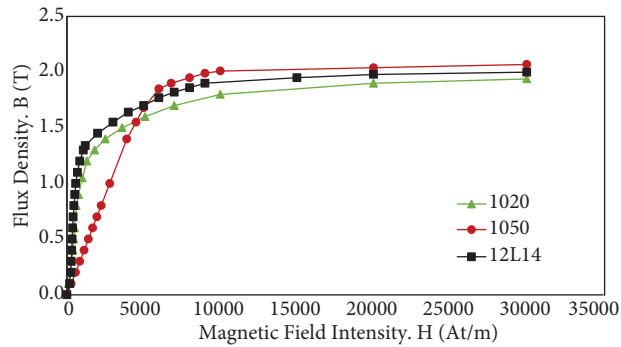
Figure 24. B–H curve for AISI 1020, AISI 1050, and AISI 12L14.
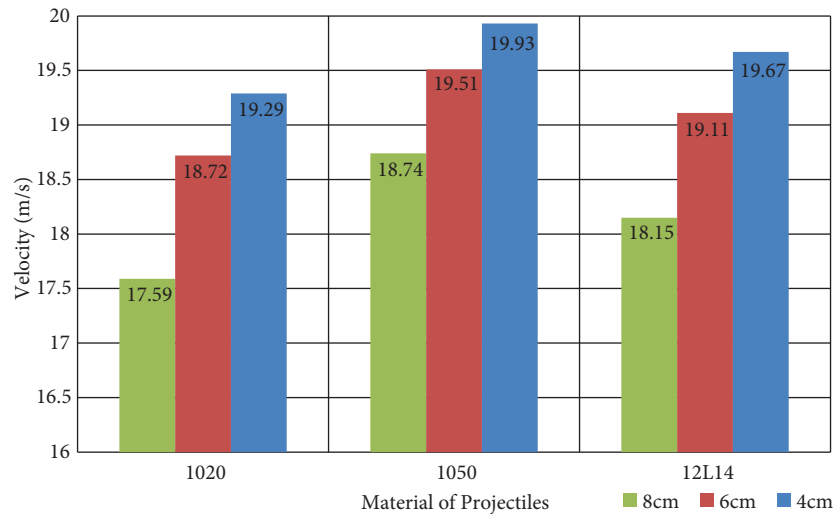
Figure 25. Velocities at 200 V.

When we consider the material type, the fastest projectiles are those constructed from 1050. 12L14 projectiles are slower than 1050 projectiles, and the slowest projectiles are the ones constructed from 1020. This is because of the difference in relative permeabilities of the three materials. The launcher has 540 turns and a current of 50 A flows through it. Then the applied magnetic field intensity becomes 27000 At/m. All of the three materials are saturated at 27000 At/m as shown in Figure 24. In order to generate a high force, the linear reluctance accelerator must be operated in the saturation zone [20]. Figure 24 shows the B–H curves for AISI 1020, AISI 1050, and AISI 12L14 [21–23]. When these curves are studied, permeabilities of the projectiles 1020, 12L14, and 1050 decrease respectively at magnetic flux values between 0 T and 0.3 T. Between 0.3 T and 1.6 T permeabilities decrease in the order 12L14, 1020, and 1050. All three materials saturate at magnetic flux densities greater than 1.6 T. Permeabilities of 1050, 12L14, and 1020 at saturation decrease. Permeability of the material at saturation must be high to have a high muzzle velocity.

The reluctance launcher is an energy conversion system. It converts electrical energy to mechanical energy. Electrical energy stored in capacitors is short-circuited by the coil and converted to magnetic energy, and then the projectile is fastened with this magnetic energy. Thus the magnetic energy is finally converted to mechanical energy. To calculate the efficiency, output energy is divided by input energy. Output of the electromagnetic launcher system is the kinetic energy of the projectile where the input of it is the electrical

energy stored in the capacitors. The efficiency of the electromagnetic launcher is given in Eq. (15) [24].

$$\eta = \frac{E_k}{E_e} = \frac{\frac{1}{2}mv^2}{\frac{1}{2}CU^2}, \tag{15}$$

where E_k is the kinetic energy of the projectile, E_e is the electrical energy stored in the capacitors, m is the mass of the projectile, v is the muzzle velocity, C is the total capacity of the capacitors, and U is the charging voltage.

Table 5. Efficiency results.

Projectile type	Projectile l length (cm)	Projectile mass (g)	Muzzle velocity (m/s)	Efficiency (%)
1020	4	36	19.29	1.55
	6	55	18.72	2.23
	8	74	17.59	2.65
1050	4	36	19.93	1.66
	6	55	19.51	2.42
	8	74	18.74	3.01
12L14	4	36	19.67	1.61
	6	55	19.11	2.32
	8	74	18.15	2.82

Total capacity of eight $2700\,\mu F$-capacitors is $21,600\,\mu F$. Charging voltage is 200V. Table 5 shows the masses, muzzle velocities of the projectiles, and the efficiency values. The highest efficiency value (3.01%) is obtained with the 8-cm 1050 projectile. If the efficiency is evaluated according to the projectile length, we see that efficiency increases when projectile length increases without taking projectile material into account. This is because of the increase in the kinetic energy of the projectile due to the increase in the mass of the projectile. If the efficiency is evaluated according to the projectile material, then it can be seen that the efficiency of 1050 projectiles is the highest. Then 12L14 and 1020 projectiles come in that order. Efficiency is one of the several important parameters that characterize the performance of a system.

As a result, the 4-cm-length projectile constructed from 1050 material has the highest velocity at 200 V. Velocity and mass of the projectile are reversely proportional. Velocity will decrease due to the increasing mass, as the length of the launched projectile increases. The projectiles that have high relative permeability will have higher velocities. The most efficient launch operation is obtained at 200 V with the 8-cm-length projectile constructed from 1050 material. Efficiency increases with the mass due to the increasing kinetic energy.

6. Conclusions

When the theoretical and experimental results are compared, it can be seen that the results are consistent with each other. The maximum velocity is achieved using projectiles built from 1050 material; then comes 12L14 and 1050 in that order in both of the studies in terms of the projectile material. The results are also consistent in terms of the projectile length. The 4-cm-length projectile reaches the maximum velocity and the velocity decreases as the length increases.

In this study, a novel result compared to the results of the past studies [13,15,24] has also been obtained. In [15], it was concluded that the maximum velocity is achieved when the projectile length is equal to the coil length. However, our study implies both theoretically and experimentally that the maximum velocity is achieved

at a projectile length that is half the coil length. Also in [15], the current applied to the coil is 1000 A whereas in our study it is 50 A. Therefore, an acceptable velocity is achieved at a significantly small current value. In [13], a 40,000 μF capacitor is charged with a voltage of 104 V and a velocity of 21.5 m/s is obtained where the efficiency of the system is 2%. In our study, the efficiency is 3.01%. In [24], a 600-V reluctance launcher is used where the maximum velocity and the maximum efficiency are 52.1 m/s and 2.87%, respectively. When compared to our study it is obvious that the voltage is high and the efficiency is low.

As a result, an easy-to-use, low-cost, portable, and structurally simple reluctance launcher that can be operated in relatively low voltage levels compared to the past studies was realized in this study.

Acknowledgment

References

[1] Bresie DA, Andrews JA. Design of a reluctance accelerator. IEEE T Magn 1991; 27: 623-627.

[2] Tomczuk B, Sobol M. Field analysis of the magnetic systems for tubular linear reluctance motors. IEEE T Magn 2005; 41: 1300-1305.

[3] Dursun M, Koç F. Linear switched reluctance motor control with PIC18F452 microcontroller. Turk J Elec Eng & Comp Sci 2013; 21: 1107-1119.

[4] Barhoumi EM, Hajji M, Salah BB. Design of a double-stator linear switched reluctance motor for shunting railway channels. Turk J Elec Eng & Comp Sci 2014; 22: 302-314.

[5] Waindok A, Mazur G. Mutual inductances in a mathematical model of the three-stage reluctance accelerator. In: 3rd International Students Conference on Electrodynamics and Mechatronics; 06–08 October 2011; Opole, Poland. New York, NY, USA: IEEE. pp. 115-118.

[6] Bayati MS, Keshtkar A, Gharib L. Analyzing the near and far field using finite difference and finite element method. IEEE T Plasma Sci 2013; 41: 1398-1402.

[7] McNab IR, Stefani F, Crawford M, Erengil M, Persad C, Satapathy S, Vanicek H, Watt T, Dampier C. Development of a naval railgun. IEEE T Magn 2005; 41: 206-210.

[8] Marder B. A coilgun design primer. IEEE T Magn 1993; 29: 701-705.

[9] Kim SW, Jung HK, Hahn SY. An optimal design of capacitor-driven coilgun. IEEE T Magn 1994; 30: 207-211.

[10] Kalender O. The optimization of launching a bullet using electromagnetic energy. PhD, Gazi University, Ankara, Turkey, 2005.

[11] Kaye RJ. Operational requirements and issues for coilgun electromagnetic launchers. IEEE T Magn 2005; 41: 194-199.

[12] Zhang C, Dong P, Duan X, Li S, Li Z, Zhang G. Analysis of reluctance coil launcher performance using coupled field-circuit method. In: International Conference on Electrical Machines and Systems; 17–20 October 2008; Wuhan, China. New York, NY, USA: IEEE. pp. 4049-4052.

[13] Slade GW. A simple unified physical model for a reluctance accelerator. IEEE T Magn 2005; 41: 4270-4276.

[14] Yadong Z, Ying W, Jiangjun R. Capacitor-driven coil-gun scaling relationships. IEEE T Plasma Sci 2011; 39: 220-224.

[15] Hou Y, Liu Z, Ouyang JM, Yang D. Parameter settings of the projectile of the coil electromagnetic launcher. 16th International Symposium on Electromagnetic Launch Technology; 15–19 May 2012; Beijing, China. New York, NY, USA: IEEE. pp. 1-4.

[16] Sen PC. Principles of Electric Machines and Power Electronics. New York, NY, USA: Wiley, 1989.

[17] Mosallanejad A, Shoulaie A. A novel structure to enhance magnetic force and velocity in tubular linear reluctance motor. Turk J Elec Eng & Comp Sci 2012; 20: 1063-1076.

[18] Ulaby FT, Michielssen E, Ravaioli U. Fundamentals of Applied Electromagnetics. 6th ed. Upper Saddle River, NJ, USA: Prentice Hall, 2010.

[19] Topbaş MA. Steel and Heat Treatment Handbook. İstanbul, Turkey: Prestij Press, 1998.

[20] Daldaban F, Ustkoyuncu N. Inductance estimating of linear switched reluctance motors with the use of adaptive neuro-fuzzy inference systems. Gazi University Journal of Science 2009; 22: 89-96.

[21] Ziegenbein J. Magnetic Clamping Structures for the Consolidation of Composite Laminates. Msc, Georgia Institute of Technology, Atlanta, GA, USA, 2011.

[22] Li F, Li X, Zhu T, Rong Y. Numerical simulation of the moving induction heating process with magnetic flux concentrator. Advances in Mechanical Engineering 2013; 2013: 1-9.

[23] An J, Kwon DS. Modeling of a magnetorheological actuator including magnetic hysteresis. Journal of Intelligent Material Systems and Structures 2003; 14: 541-550.

[24] Xiang H, Lei B, Li Z, Zhao K. Design and experiment of reluctance electromagnetic launcher with new-style armature. IEEE T Plasma Sci 2013; 41: 1066-1069.